



Full Text View

[Volume 30, Issue 7 \(July 2000\)](#)

Journal of Physical Oceanography

Article: pp. 1514–1531 | [Abstract](#) | [PDF \(660K\)](#)

Eddy Shedding from a Boundary Current around a Cape over a Sloping Bottom

C. Cenedese*

Department of Applied Mathematics and Theoretical Physics, University of Cambridge, Cambridge, United Kingdom

J. A. Whitehead

Physical Oceanography Department, Woods Hole Oceanographic Institution, Woods Hole, Massachusetts

(Manuscript received October 22, 1998, in final form May 21, 1999)

DOI: 10.1175/1520-0485(2000)030<1514:ESFABC>2.0.CO;2

ABSTRACT

The authors discuss laboratory experiments that elucidate the mechanism of formation and westward drift of anticyclonic baroclinic vortices from a buoyant surface current flowing along a lateral boundary and around a cape. Experiments were carried out with a sloping bottom in order to simulate the topographic β effect. They showed how a vortex can be generated from the current where it separates and reattaches to the cape and that, under some conditions, the eddy is able to detach from the cape and drift westward following isobaths. Two important timescales regulate the flow: the time t_f that the current takes to generate a vortex and the time t_d that the vortex takes to drift westward for a distance equal to its radius. When these two timescales are either of the same order of magnitude or $t_f < t_d$, the eddy was observed to translate westward. For $t_f > t_d$ the vortex was able to form at the cape but it did not detach and drift westward. The influence of the depth of the lower layer, h_0 , on the flow was investigated. The theoretical westward speed U_{2d} depends on the depth of the lower layer: the deeper the lower layer the slower the drift. The values of the slope s required in the experiments in order to obtain the detachment and drift of the vortex indicate that the phenomena will occur on a planetary β plane only when the variation of the Coriolis parameter with latitude is reinforced by a topographic β effect. A good agreement between the laboratory experiments and the observations of meddies in the Canary Basin, where the Mediterranean Outflow from the Strait of Gibraltar flows along the coast of Spain and around Cape St. Vincent, suggests that the eddy-shedding process is similar to that observed in the laboratory experiments.

Table of Contents:

- [Introduction](#)
- [The experiments](#)
- [Eddy-shedding mechanism](#)
- [Mechanism for westward](#)
- [Qualitative results](#)
- [Quantitative results](#)
- [Comparison with observation](#)
- [The planetary \$\beta\$](#)
- [Conclusions](#)
- [REFERENCES](#)
- [APPENDIX](#)
- [TABLES](#)
- [FIGURES](#)

Options:

- [Create Reference](#)
- [Email this Article](#)
- [Add to MyArchive](#)
- [Search AMS Glossary](#)

Search CrossRef for:

- [Articles Citing This Article](#)

Search Google Scholar for:

- [C. Cenedese](#)
- [J. A. Whitehead](#)

1. Introduction

In the last 10 years several surveys in the Canary Basin of the eastern Atlantic have shown the presence of Mediterranean Water in lens-shaped vortices called “meddies.” These eddies were observed to form primarily near Cape St. Vincent ([Bower et al. 1997](#)) and to rotate anticyclonically ([Armi and Zenk 1984](#); [Pingree and Le Cann 1993](#)). The continuous Mediterranean outflow through the Strait of Gibraltar develops into a coastal current along the coast of Spain and Portugal and provides the water found within the meddies. The mechanism by which this continuous outflow breaks into discrete coherent vortices is not clear.

Meddies are characterized by their high salinity and temperature relative to the surrounding water and have a radius of approximately 50 km, a vertical extent of about 1 km, a core depth in the range 1100–1200 m, and are approximately symmetric about a horizontal plane passing through the core. The azimuthal velocity of these lenses is approximately 0.2 m s^{-1} at radii between 30 and 45 km. Their main direction of propagation is generally southward and they are observed to be long-lived structures ([Armi et al. 1988](#)). Two dimensionless parameters are important for this kind of flow: the Rossby number $Ro = \zeta/f$, where ζ is the relative vorticity and f is the planetary vorticity, and the Burger number $B = (g'H)^{0.5}/fL$, where g' is the reduced gravity, H is the fluid depth, and L is a characteristic horizontal lengthscale. A low Rossby number suggests that the flow is in quasigeostrophic balance (the buoyancy forces and the Coriolis forces are in balance), whereas a Burger number of order of unity indicates that the horizontal scale of the eddy is of the same order of magnitude as the Rossby radius of deformation. For the meddies these parameters take values approximately $Ro \approx 4 \times 10^{-2}$ and $B \approx 2$. Using a Brunt–Väisälä frequency of $N = 10^{-3} \text{ s}^{-1}$ and a shear $\partial u/\partial z$ of $4 \times 10^{-4} \text{ s}^{-1}$, the Richardson number $Ri = N^2/(\partial u/\partial z)^2 = 6$ so turbulence is negligible for this kind of flow. Moreover the meddies last for years indicating that viscous decay times are very long.

The evolution and translation of eddies on a sloping bottom or a β plane is a problem of particular importance because of its relevance to the transport of water in boundary currents and mingling of this water with the ocean interior. The completely barotropic flow of an isolated eddy on the β plane was discussed by [Stern \(1975\)](#), who showed how this flow can have a steady solution only if it is composed of a coupled cyclone–anticyclone system called a “modon.” A model of cold eddies migrating on a sloping bottom was given by [Nof \(1983\)](#); the eddy was predicted to travel to the west with a characteristic velocity given by $U_d = g's/f$, where s is the slope of the bottom. Water in the lens circulated anticyclonically and the deep upper layer was motionless. Later experimental and theoretical studies by [Mory \(1985\)](#), [Mory et al. \(1987\)](#), and [Whitehead et al. \(1990\)](#) indicated that similar eddies can be produced on a sloping bottom in laboratory experiments but that the eddies were qualitatively different from the Nof solution. The eddies produced in the laboratory always involved motion in an active upper layer characterized by a strong cyclonic circulation. A more general expression for the westward drift was given by [Cushman-Roisin et al. \(1990\)](#) and the previous results can be expressed as asymptotic limits to this single solution. Theoretical studies by [Swaters \(1991\)](#), and numerical simulations by [Davey and Killworth \(1989\)](#), [Jiang and Garwood \(1996\)](#), and [Jungclauss \(1999\)](#) illustrate some additional aspects of eddies over a sloping bottom or a β plane but do not recover the migration of the eddy away from a current flowing along a vertical wall. In a recent theoretical study [Pichevin and Nof \(1996\)](#) showed how the integrated momentum associated with any steady current that curves around a cape cannot be balanced without generating and shedding eddies. Their study suggested the geometry of the experiments conducted here.

In this paper we discuss laboratory experiments that elucidate the mechanism of formation and westward drift of anticyclonic baroclinic vortices from a buoyant surface current flowing along a lateral boundary and around a cape. This model simplifies a number of important features of the oceanic flow (i.e., meddies are interior features) and it is necessary to understand whether they play any part in the meddy formation and drift processes. The buoyant vortices are influenced by a sloping bottom through an active lower layer and vortex stretching. The lower layer in turn influences the upper-layer vortex through advection of vorticity, leading to motion of the upper-layer eddy along the depth contours. The upper half of a submerged meddy is missing in this model, but the important contributions of a sloping bottom and the baroclinic interface slope are included. The motion along the bottom slope is related to westward motion on a planetary β plane. The influence of a sloping bottom topography on the westward drift of buoyant baroclinic eddies was previously investigated in a one-layer reduced-gravity and two-layer environment by [Linden \(1991\)](#) and [Cenedese and Linden \(1999\)](#), respectively. Vortices were produced by a continuous source of less dense fluid, and regimes with differences in the flow behavior and in the westward propagation speeds were observed.

The experimental apparatus is described in [section 2](#) and the eddy shedding and drift mechanism are discussed in [sections 3](#) and [4](#), respectively. Qualitative results are presented in [section 5](#) and quantitative results are given in [section 6](#). Comparison with oceanographic observation are presented in [sections 7](#) and [8](#) and the conclusions are discussed in [section 9](#).

2. The experiments

A sketch of the apparatus is shown in [Fig. 1](#) and an overview of the experimental parameters and measured quantities is shown in [Table 1](#). The experiments were conducted in a glass tank of depth 60 cm and base 61 cm. This was mounted on a direct-drive, diameter 1 m, rotating turntable with a vertical axis of rotation. We used a square tank to avoid optical distortion from side views associated with a circular tank. The tank was centered on the vertical rotation axis of the table and had a bottom slope (s) to simulate the β effect. The use of a sloping bottom to represent a β plane is strictly valid only for a unstratified fluid. In the two-layer stratification used here, the slope provides an equivalent potential vorticity (PV) gradient in the lower layer, but there is not a direct representation of the PV gradient in the upper layer. Nevertheless, the thermal wind coupling across the interface implies that the motion in the upper layer is also influenced by the lower-layer PV gradient. Hence, the essential features of a β plane are captured using a slope in this case where the shallowest part of the tank corresponded to the “northern” shore of the Northern Hemisphere topographic β plane. East was to the right looking onshore, west was to the left, and south was the deepest end. The tank was filled with salty water of density ρ_2 . A vertical sheet of Perspex 20 cm long and 1 cm wide was placed perpendicular to the eastern wall of the tank in order to model the effect of a cape. The depth of the salty water at the cape, h_0 , varied between 14.0 and 24.7 cm. A reservoir R_1 of fresh dyed water of density $\rho_1 < \rho_2$ was connected to a nozzle via a peristaltic pump and a plastic tube. The nozzle was covered by a piece of sponge. This source was located against the eastern wall of the tank, a few millimeters under the free surface and 14 cm from the cape. The outlet was directed up the slope so that the turbulent jet of buoyant water would reach the cape and there develop into a buoyancy-driven current along the cape. However, the current was observed to retain some momentum after reaching the cape, and we will discuss in detail the effects of the source momentum flux on the flow in [section 6c](#). The jet was forced by a constant flow rate $Q = 8.7 \text{ cm}^3 \text{ s}^{-1}$. Mixing between the source and the surrounding waters occurred along the interface of the two layers. The mixing was confined between the jet and the cape. The buoyancy forces are described by the reduced gravity $g' = g(\rho_1 - \rho_2)/\rho_1$, where g is the gravitational acceleration. A considerable reduction of the value of g' was observed where the mixing occurred, between the source and the cape, and the flow rate at the cape increased (in order to conserve buoyancy flux, see [section 6c](#)). In the experiment the buoyant water from the source was characterized by $g' = 1.00 \text{ cm s}^{-2}$ while samples of the water in the current downstream of the region near the source, after a significant amount of mixing had occurred, gave values of approximately $g' = 0.60 \text{ cm s}^{-2}$. The Coriolis parameter f was varied from 0.22 s^{-1} to 1.37 s^{-1} and the slope s of the bottom was set at five different values $s = 0.26, 0.38, 0.50, 0.62, \text{ and } 0.76$. These parameters produce a typical spindown time for the ambient fluid of $t = h_0/(vf)^{0.5} = 140 \text{ s}$ (using $h_0 = 14 \text{ cm}$ and $f = 1 \text{ s}^{-1}$). This is longer than the detachment time of roughly 100 s or less reported in [section 5](#) for these parameters. In addition, the spindown time of the baroclinic eddies will be very much longer.

A video camera was mounted above the tank and fixed to the turntable so that velocity measurements could be obtained in the rotating frame. The current was made visible by dyeing the source water with food coloring and by adding buoyant paper pellets on the surface. The lower-layer flow was observed by injecting dyed tracer with a syringe positioned on the southeast side of the cape. The motion of dye was also observed both from top and side views.

The velocities were measured by tracking the paper pellets on the surface. A computer system with a frame-grabber card and the image processing software DigImage ([Dalziel 1992a](#)) was used to acquire and process the images from the video records of the flow. The video tape was recorded with a time lapse of 12 seconds and was scan converted from MTS to PAL format. The conversion and the time lapse contributed to errors in calculating the velocity and vorticity fields. Typically less than 500 paper pellets were located in each frame and the velocities obtained by sampling the video film at a frequency of approximately 2 Hz. Automatic matching of these locations to the ones in previous frames produced the tracking files. Particle velocities were calculated over five samples and the velocity field was obtained by mapping the individual velocity vectors onto a rectangular grid using a spatial averaging over 6.2 cm, and averaging over 24 s. The vorticity was calculated from these gridded velocity data. The error in the velocities is estimated to be somewhat larger than 5% quoted by [Linden et al. \(1995\)](#), whereas the error in the derived fields is estimated to be larger than 10% (for details see [Dalziel 1992b, 1993](#)).

3. Eddy-shedding mechanism

In order to understand the mechanism involved in the detachment of an eddy from the current and its consequent shedding, we calculate the timescales of the formation of an eddy from a buoyant current flowing around a cape and compare it with a timescale for the drift of the eddy.

The formation timescale t_f is defined as the time for the volume V of the eddy to be filled by buoyant fluid flowing at a flow rate Q . The eddy is considered to be a zero potential vorticity paraboloid and hence its volume can be expressed as

$$V = \frac{\pi R^2}{2} = \frac{\pi R^2}{2f^2}, \quad (1)$$

where the radius of the vortex R is taken to be equal to the Rossby radius of deformation $R_D = (g'(h_v h_2)^{1/2})^{1/2}/f$ based on the geometric mean of the vortex depth h_v and the lower-layer depth underneath it $h_2 = h_0 - sr \sin\theta - h_v$, both calculated at $r = 0$ (Fig. 2 \bullet); experimental results indicate that this is a reasonable measure of the vortex radius (section 6c). In order to calculate the time for filling the volume V two assumptions are introduced. First, the maximum depth of the vortex is considered to be equal to the maximum depth of the current. Second, the maximum current depth (which occurs at the wall) is calculated assuming that the current is in geostrophic balance. The first approximation will be experimentally verified later and the second will be discussed further in section 6c. Using the subscripts c and v to indicate quantities related to the current and to the upper-layer vortex, respectively, the geostrophic balance for the current along the eastern wall gives

$$fv_c = g' \frac{\partial h_c}{\partial x}. \quad (2)$$

This leads to

$$Q = \int_0^x v_c h_c dx' = \int_0^x \frac{g'}{f} \frac{\partial h_c}{\partial x'} h_c dx' = \frac{g' h_c^2}{2f}, \quad (3)$$

where x is the alongslope coordinate normal to the eastern wall. Consequently,

$$h_v \approx h_c = \sqrt{\frac{2fQ}{g'}}. \quad (4)$$

Using (1) and (3) the formation time is then given by

$$t_f = \frac{V}{Q} \approx \frac{\pi \sqrt{h_v h_2}}{f h_v} = \frac{1}{4} T \frac{\sqrt{h_v h_2}}{h_v}, \quad (5)$$

where T is a rotation period. This predicted formation time is quite small, indicating that probably not all the assumptions made are correct (see section 6c), in particular geostrophy is questionable since it supposes the flow to be steady, although the force balance it represents is probably the main one. However, the value t_f measured during laboratory experiments, even if systematically larger than (5) (see Fig. 15 \bullet), is still of the same order of magnitude. Therefore (5) serves as a good starting point to understand the basic mechanism of vortex formation and drift from a cape.

The timescale for the westward drift of the eddy over a length equal to the radius of the vortex is calculated assuming that the westward drift velocity U_d scales with the long Rossby wave speed given by $U_d = g's/f$ (Nof 1983). (This velocity is a first approximation and modifications are discussed in sections 4 and 6c). Hence

$$t_d = \frac{R}{U_d} = \frac{1}{s} \left(\frac{\sqrt{h_v h_2}}{g'} \right)^{1/2}. \quad (6)$$

When the timescale for the formation of the vortex and the timescale for the westward drift are of the same order of magnitude ($t_f \cong t_d$), a vortex will form at the cape and then detach from it as a result of a westward drift. Using (5) and (6) we can find

$$\frac{t_f}{t_d} = \frac{\pi s R}{h_v} \cong 1. \quad (7)$$

More generally, we define $s' = h_v/R$ as the slope associated with the interface displacement generated by the vortex, which can also be expressed as a function of the external variables using (4) and the usual expression for the Rossby radius

R_D to give

$$s' = \frac{(2Q)^{3/8} f^{11/8}}{g'^{7/8} [h_0 - (2fQ/g')^{1/2}]^{1/4}}. \quad (8)$$


Equation (7) implies that when the slope of the topography is of the same order of magnitude as the slope of the vortex interface displacement, the eddy will detach and drift westward. In the present analysis we will only consider relatively large slopes with $s \geq 0.25$. No shedding was observed for slopes $s < 0.25$ and this case will be discussed separately in [section 8](#).

Two other possible situations can occur when t_f is bigger or smaller than t_d so that

$$\frac{t_f}{t_d} < 1 \Rightarrow s < \frac{s'}{\pi}, \quad \frac{t_f}{t_d} > 1 \Rightarrow s > \frac{s'}{\pi}. \quad (9)$$

In the first case the formation process is faster than the drift process. Consequently, the eddy will grow to its final volume V and then drift westward after interacting for a short time with the vortex that is forming next. In the second case the time for the formation of the vortex is longer than the time necessary for its drift so that some fluid from the vortex can drift westward before the formation process of the vortex is completed. Therefore, the vortex takes even longer to reach its final volume V and cannot drift as a coherent structure but instead remains attached to the cape. In conclusion we predict that an efficient vortex separation from the current and westward drift only occurs when $t_f/t_d \leq 1$ and therefore the topographic slope is smaller than the interfacial slope scaled by π , while the process is inefficient whenever the formation timescale is larger than the drift timescale ($t_f/t_d > 1$).

4. Mechanism for westward drift

Consider a buoyant vortex at the free surface of a homogeneous layer having a sloping bottom topography as sketched in [Fig. 2](#) , where in polar coordinates the depth of the ambient fluid underneath the vortex is $h_2 = h_0 - sr \sin \theta - h_1$. A first approximation of the resulting flow can be obtained by neglecting the effect of friction on all surfaces (the density interface, the free surface, and the tank bottom). The inviscid flow, both inside and outside the vortex, is governed by the conservation of potential vorticity. The continuity equation in the upper layer is


$$\frac{\partial(ru_1 h_v)}{\partial r} + \frac{\partial(v_1 h_v)}{\partial \theta} = 0 \quad (10)$$

and in the lower layer is

$$\frac{\partial(ru_2 h_2)}{\partial r} + \frac{\partial(v_2 h_2)}{\partial \theta} = 0, \quad (11)$$

where u_1 (u_2) and \mathbf{v}_1 (\mathbf{v}_2) are the radial and azimuthal velocity in the upper (lower) layer.

a. Lower-layer vortex

The upper-layer vortex formation squashes the fluid column underneath so that, in order to conserve potential vorticity, the fluid in the column will start rotating clockwise in an anticyclonic motion. Consider a circular lower-layer anticyclonic vortex with azimuthal velocity \mathbf{v}_2 and the same radius R as the vortex in the upper layer ([Fig. 2](#) ). In the absence of a zonal drift and assuming the radial velocity to be negligible, the lower-layer continuity [equation \(11\)](#) becomes

$$\frac{\partial(v_2 h_2)}{\partial \theta} = 0. \quad (12)$$

Applying this to the north (N) and south (S) sides of the eddy yields

$$\mathbf{v}_{2N} h_{2N} \approx \mathbf{v}_{2S} h_{2S}. \quad (13)$$

where

$$h_{2N} = h_0 - sR - h_{vN}, \quad h_{2S} = h_0 + sR - h_{vS}. \quad (14)$$

If the same fluid circulates around the eddy without loss of mass and $h_{2N} \neq h_{2S}$, we conclude that $\mathbf{v}_{2N} \neq \mathbf{v}_{2S}$. This discrepancy is at the base of the arguments of [Bjerknes and Holmboe \(1944\)](#), [Rossby \(1948\)](#), and [Cushman-Roisin et al. \(1990\)](#), who consider a variable Coriolis parameter ($f = f_0 + \beta y$) instead of a variable depth ($h_2 = h_0 - sr \sin\theta - h_v$). The Coriolis forces associated with these two velocities will no longer balance each other and, assuming the vortex shape is unchanged, the addition of a zonal westward velocity U_{2d} is required in order to reach equilibrium. The vortex will initially move southward for an inertial lengthscale proportional to the velocity difference. This motion will induce a Coriolis force westward. Consequently, the vortex will be deflected westward until the Coriolis force associated with the westward drift velocity balances the net Coriolis force associated with the difference between \mathbf{v}_{2N} and \mathbf{v}_{2S} . This transient regime takes place for a timescale of the order of one inertial period. After reaching a steady balance the Coriolis forces in the north and south side must be equal; that is,

$$f(\mathbf{v}_{2N} - U_{2d}) = f(\mathbf{v}_{2S} + U_{2d}). \quad (15)$$

This gives the result that

$$\mathbf{v}_{2N} = \mathbf{v}_{2S} + 2U_{2d}. \quad (16)$$

Substituting [\(16\)](#) into [\(13\)](#) yields

$$(\mathbf{v}_{2S} + 2U_{2d})h_{2N} = \mathbf{v}_{2S}h_{2S}, \quad (17)$$

and using [\(14\)](#)

$$U_{2d} = \frac{\mathbf{v}_{2S}(2sR + h_{vN} - h_{vS})}{2(h_0 - sR - h_{vN})}. \quad (18)$$

Assuming for simplicity that h_{vN} and h_{vS} are much smaller than sR and that h_{vN} and sR are much smaller than h_0 , [\(18\)](#) becomes

$$U_{2d} = \frac{\mathbf{v}_{2S}sR}{h_0}, \quad (19)$$

where the zonal velocity has exactly the same expression as in [Cushman-Roisin et al. \(1990\)](#) if the variable depth is substituted for the variable Coriolis parameter. For anticyclones the zonal velocity is directed westward while it is easy to follow the same procedure and show that for cyclonic vortices an eastward zonal velocity U_{2d} is required in order to reach equilibrium.

b. Lower- and upper-layer interaction

We will assume that the lower-layer vortex interacts with the upper-layer vortex through thermal wind balance across the interface ([Griffiths and Hopfinger 1986, 1987](#)). The lower-layer vortex drifts westward as discussed in [section 4a](#) and its vorticity field induces the drift of the upper-layer vortex at the same speed $U_{1d} = U_{2d}$. Any small departure of the upper-layer vortex from a configuration concentric with the lower-layer motions will be removed through advection by the lower-layer velocity field. This process is similar to the ‘‘axisymmetrization’’ of vortices in a fluid of uniform depth and subjected to a uniform f , but in the present case the vortex on a slope will not be circular.

In order to calculate the lower-layer azimuthal velocity and consequently the westward velocity U_{2d} , we will use conservation of potential vorticity in both layers. In the top layer we assume that the eddy is generated by an inflow from the coastal current having zero potential vorticity and, consequently, the vorticity is given by $\zeta_v = -f$. In the lower layer

$$n_0 = sR \sin\theta \quad n_0 = sR \sin\theta = n_v$$

where we assume no movement of the lower-layer column up- or downslope. A first approximation to the relative vorticity becomes

$$\zeta_2 \cong -\frac{fh_v}{h_0}. \quad (21)$$

If we consider that the vortices in the lower- and upper-layer have approximately the same radius, then the ratio of the two vorticities gives a scale of the ratio of the azimuthal velocity in the two layers. The ratio of the two velocities is then given by

$$\frac{\zeta_2}{\zeta_v} \approx \frac{v_2}{v_v} = \frac{h_v}{h_0}. \quad (22)$$

Integration of the vorticity in the upper layer leads to the anticyclonic azimuthal velocity $\mathbf{u}_v = fR/2$. Using (22) to obtain \mathbf{u}_2 and assuming for simplicity that $\mathbf{u}_{2s} = \mathbf{u}_2$, then (19) yields a westward velocity drift given by

$$U_{2d} = \frac{1}{2} \frac{g's\sqrt{h_v h_2}}{f} \frac{h_v}{h_0^2}. \quad (23)$$

The drift velocity (23) is directed westward for anticyclones and eastward for cyclones and this is in contradiction with the laboratory observations discussed in section 5b of a westward drift for both cyclones and anticyclones. A different explanation is required for this behavior.

c. Drift due to induced vorticity

A β gyre approach can be applied to fluid columns within the vortex and another contribution to the westward drift velocity can be found. A vortex on a slope advects fluid columns both upslope and downslope regardless of the sign of the vorticity and regardless of whether or not the vortex is drifting. Conservation of potential vorticity dictates that the columns advected upslope and downslope acquire anticyclonic and cyclonic relative vorticity, respectively. The vorticity ζ of these columns is given by

$$\zeta = \mp \frac{sRf}{h_0}. \quad (24)$$

These regions of positive and negative vorticity form a dipolar contribution to the velocity field, which can then induce motion “westward” along the slope (Fig. 3). The same mechanism was investigated by Cushman-Roisin et al. (1990) where, instead of a variable depth, a variable Coriolis parameter was investigated. Writing the azimuthal velocity associated with the induced vorticity as \mathbf{v}' , we have $\mathbf{v}' = \zeta R/2$. The westward drift of the vortex due to the induced dipolar vorticity component is given by

$$U_{2d} = 2v' = \frac{g's}{f} \frac{\sqrt{h_v h_2}}{h_0}. \quad (25)$$

This expression for the westward velocity is exactly the same as in Cushman-Roisin et al. (1990) if the variable depth is substituted for the variable Coriolis parameter, although it is derived with a different approach. In appendix 1 the same expression for U_{2d} is derived using the approach described in Cushman-Roisin et al. (1990).

The two different drift mechanisms discussed in sections 4a–c are not linear processes; therefore, the two contributions to the westward drift velocity given by (23) and (25) cannot be strictly added together to give the total westward velocity. However, in order to find an approximation for the total westward speed we will simply add the two terms together, being aware that is not strictly correct. For an anticyclonic vortex

$$U_{2dTOTAL} = \frac{g's}{f} \frac{h_0}{h_0} \left[1 + \frac{1}{2} \frac{h_v}{h_0} \right], \quad (26)$$

and for a cyclonic vortex

$$U_{2dTOTAL} = \frac{g's}{f} \frac{\sqrt{h_v h_2}}{h_0} \left[1 - \frac{1}{2} \frac{h_v}{h_0} \right], \quad (27)$$

where, for the experiments described in section 5, the second term on the right side of the equations is only 28% of the first term on the right side of the equations. Therefore the induced-dipole mechanism leading to (25) is the primary cause of the westward drift. In any case, (26) will be compared in section 6a to experimental results as a test of its validity.

5. Qualitative results

In the experiments the buoyant current generated by the jet on the eastern wall propagated upslope (northward) until it encountered the cape. It rounded the cape and turned eastward after separating from the corner and reattaching to the cape some distance from the tip. Providing the current had a large enough volume flux, under some conditions, it eventually detached from the cape and drifted westward. Experiments carried out with a different type of source providing less volume flux than the jet source, and experiments with lower flow rate showed both that the eddy formation mechanism was inhibited and that the current reattached at the cape without forming a region of closed streamlines at the cape.

We first varied only the slope s and the Coriolis parameter f in order to observe eddy shedding as discussed in section 3. The influence of lower-layer depth and of bottom topography was investigated for some of these experiments. A different orientation of the cape relative to the direction of the bottom slope was also investigated in order to simulate different geographical situations.

a. Eddy shedding

Experiments were carried out with different slopes and for each of those we varied the Coriolis parameter in order to investigate different values of the dimensionless parameter s'/π (8), as shown in Fig. 4. The lower-layer depth at the cape was kept constant and approximately equal to 15 cm. For $s > s'/\pi$ the current streamlines separated from the corner and formed an anticyclonic vortex that started growing slowly at the cape. Some of the fluid within the vortex leaked out and drifted westward along an isobath (Fig. 5a). The formation time of the vortex was very long and no eddy shedding was observed. For some values of $s > s'/\pi$, when the value of the slope was $s = 0.76$ (the largest used) and $s = 0.62$, the eddy was observed to detach after a timescale much longer than for the regime characterized by clear eddy shedding ($s \lesssim s'/\pi$) and we refer to these conditions as the transient regime. The detachment also involved the destruction of the anticyclonic eddy due to baroclinic or shear instabilities growing at the front of the eddy. For $s \lesssim s'/\pi$ the current flowing around the cape formed an eddy after streamlines separated from the wall (Fig. 5b). Before the streamlines reattached to the cape, the flow passed through a stagnation point. Beyond this point the streamlines in the outer edge of the current reattached to the cape, evidently influenced strongly by depth contours, while the streamlines in the inner part of the current closed on themselves at the end of the cape. The closed streamlines indicated the presence of the anticyclonic vortex (Fig. 6a), and this grew in size due to the continuous inflow from the current.

After a time the stagnation point moved westward along the cape until it reached the tip of the cape. The vortex then separated from the current and from the cape (Figs. 6b,c,e). The current streamlines then reestablished their previous path with separation at the cape and reattachment downstream, starting the whole process again and leading to the production of a new vortex (Figs. 6c,d,e). After each eddy detached from the current it drifted westward approximately following isobath contours. The vortex generally lost its axisymmetric shape and coherency and could be destroyed before reaching the western wall of the tank (as a result of processes discussed below).

b. Instability processes

Instability was observed to influence the formation and drift of eddies as well as the flow of the boundary current along the side boundary and around the cape. These instabilities are expected to range from those that were almost purely baroclinic and driven by the release of potential energy to those that are almost purely barotropic and which drew on the kinetic energy in the basic shear flow. However, the appearance of amplified disturbances is expected to be similar for both types of instability and, therefore, it was difficult to determine which one was occurring or was dominant. As observed by Griffiths and Linden (1981), these instabilities led to both vortex splitting and rapid radial spreading of the water of the upper-layer eddy. At an early stage of the instability, cyclonic rings, or "spiral arms," of buoyant fluid were produced,

indicating the presence of cyclonic vortices in the lower layer.

The anticyclonic eddies were destroyed as a result of two different processes. The first process occurred only in a few experiments where the boundary current was observed to become unstable along the southern side of the cape, with backward breaking wave crests. The buoyant fluid started meandering, with anticyclonic relative vorticity created within the meander crests and cyclonic relative vorticity produced in the lower layer (due to stretching of water columns) in the meander troughs. The cyclonic motion trapped some of the buoyant fluid and formed visible cyclonic arms that gave the appearance of backward breaking waves (Fig. 7a). When each of these cyclonic vortices reached the tip of the cape they interacted with the anticyclonic vortex generated at the tip by the current. The two structures began moving westward as a dipole in which the anticyclone initially had the greater intensity. Thus the anticyclone advected the cyclone slightly southward to deeper water so that the lower-layer cyclone was stretched, further increasing its intensity. Eventually the circulation intensity of the cyclone overcame the anticyclone circulation and it entrained fluid from the anticyclone, elongating and destroying it.

The second process was observed in almost all experiments where the anticyclonic vortex detached, as a single structure, from the current and drifted westward. Eventually, the anticyclone became unstable and formed two spiral arms (Figs. 7b and 6e) as a result of the generation of local cyclonic vorticity in the lower layer by baroclinic instability as shown by the dark dye tracer positioned in the lower layer. One of the cyclonic vortices was advected southward by the anticyclone and increased its intensity until it became strong enough to tear the anticyclone apart as shown in Fig. 6f. This kind of instability has been observed also when the vortex was generated by a point source in a two-layer environment (Cenedese and Linden 1999) or a one-layer environment (Linden 1991). Figure 4b (Cenedese and Linden 1999) shows two anticyclonic vortices moving westward over a sloping bottom, and it is clear that the vortex on the left of the figure has an elongated shape with formation of spiral arms similar to the vortex on the left of Fig. 6e. The instability of anticyclonic vortices over a flat bottom has been previously investigated by Griffiths and Linden (1981) and, as in Fig. 6e, $n = 2$ was observed to be the minimum azimuthal wavenumber for an unstable disturbance.

c. The influence of depth

The depth of the lower layer plays the important role of determining the magnitude of the relative vorticity produced in the lower layer by squashing of the lower-layer column underneath the upper-layer eddy and stretching and squashing due to the bottom slope. The topographic β effect depends on the lower-layer depth through the relation $\beta = sf/h_0$. In this section we will discuss only the influence of h_0 on the eddy shedding mechanism under the restriction that the β effect associated with the bottom slope remains unchanged. Pairs of experiments were carried out with the same value of the Coriolis parameter but varying the lower-layer depth and the slope to give the same effective β , namely

$$\beta = \frac{s_A f}{h_{0A}} = \frac{s_B f}{h_{0B}}, \quad (28)$$

where the subscripts A and B label the two experiments with $h_0 = 15$ cm and $h_0 = 23$ cm, respectively. The value of the dimensionless parameter s'/π depends only on f and h_0 for a given flow rate and reduced gravity, and for both experiments s'/π was chosen to be larger than s in order to observe the shedding of eddies. The flow structure of experiment A has already been discussed in section 5a. During experiment B the vortex formed at the cape but it did not detach, so it had a similar appearance as the flow presented in section 5a for $s > s'/\pi$. In the two experiments the westward drift was forced by the same topographic β effect. Therefore the different behavior observed was caused by the increase of the lower-layer depth and the relative decrease of the lower-layer column squashing by the eddy. These give a lower value for the westward drift velocity (26).

d. The influence of the “cape” position

Experiments were performed with different orientations of the cape relative to the direction of bottom slope in order to obtain a more complete view of possible scenarios along real coastlines. We positioned the cape perpendicular to the western wall of the tank with a buoyant coastal current encountering the cape from the north (Fig. 8a). After encountering the cape the current flowed around it and then turned westward separating from the corner and reattaching itself to the cape. An anticyclonic vortex formed at the cape in the same way as in the previous experiments and was observed to remain in its initial position for $s > s'/\pi$. For $s \leq s'/\pi$ the eddy migrated westward and merged with the current flowing around the cape and along the western wall. As expected, no eddies were observed to cross the tank in the eastward direction. Nor were eddies shed when the cape was positioned orthogonal to the southern wall (Fig. 8b). In this geometry some fluid from the current leaked westward just before going around the cape. Consequently the vortex did not form completely nor was it shed from the cape.

In other experiments the cape was orientated perpendicular to the northern wall with a current flowing westward (Fig. 8c). This geometry, where the cape was perpendicular to the isobaths, was an attempt to simulate a peninsula on a shelf with a strong offshore slope. The resulting flow showed similar behavior to those described in section 5a, with the eddies migrating westward along isobaths for values of $s \lesssim s'/\pi$. It appears that the results for the geometry with the cape positioned perpendicular to the eastern wall apply to this case as well.

6. Quantitative results

a. Westward drift

The westward drift speed was measured for the experiments in which $s \lesssim s'/\pi$ and in Fig. 9 it is plotted against the predicted drift speed (26) calculated in section 4c. This theoretical speed has been calculated considering a single baroclinic vortex drifting westward over a sloping bottom, therefore the poor agreement between the theory and the experiment shown in Fig. 9 could be due to eddy–eddy interaction occurring at the cape as observed during the laboratory experiments. Experiments designed to produce a single vortex over a slope would test the theory better. However, the theoretical speed (26) is an improvement with respect to the long Rossby wave speed given by $U_d = g's/f$ (Nof 1983) that is strictly valid only for a cold eddy migrating on a sloping bottom with a deep motionless upper layer. When both layers are active a correction to this speed including the two-layer depths and their azimuthal velocity is needed.

b. Velocity and vorticity fields

For the experiments in which $s \lesssim s'/\pi$, the current flowed around the cape and an anticyclonic vortex grew where the current separated, as described in section 5a. The velocity and vorticity fields show that the maximum anticyclonic vorticity occurred at the center of each vortex and decreased outward. The vortex was then observed to detach and drift westward and a new vortex started growing at the cape. The first vortex drifted westward as an independent structure, as shown in Figs. 10b and 10c, and its velocity and vorticity decreased in time as a result of dissipation (due principally to the instabilities discussed in section 5b). Patches of cyclonic vorticity were visible on the sides of the vortex when it was approaching the western wall. The cyclonic vorticity reveals the presence of cyclonic motion in the lower layer due to instability processes that led to both vortex splitting and rapid radial spreading of the water of the upper-layer eddy as shown in Fig. 10e. The second vortex started growing at the cape and eventually detached from it in an analogous fashion to the first vortex (Figs. 10c and 10d). During the westward drift the velocity and vorticity fields associated with each vortex were completely separated from those of the next vortex and fluid with approximately zero velocity and vorticity was found between two consecutive vortices (Fig. 10d). The current flowing around the cape was observed to move along the eastern and northern wall with an approximately constant speed.

The autocorrelations of the east–west (zonal) and north–south (meridional) component of the velocity,

$$R_{uu} = \frac{\overline{u(t)u(t + \Delta t)} - \overline{u(t)}\overline{u(t + \Delta t)}}{\sqrt{\overline{u(t)^2} - \overline{u(t)}^2}\sqrt{\overline{u(t + \Delta t)^2} - \overline{u(t + \Delta t)}^2}}, \quad (29)$$

$$R_{vv} = \frac{\overline{v(t)v(t + \Delta t)} - \overline{v(t)}\overline{v(t + \Delta t)}}{\sqrt{\overline{v(t)^2} - \overline{v(t)}^2}\sqrt{\overline{v(t + \Delta t)^2} - \overline{v(t + \Delta t)}^2}}, \quad (30)$$

were calculated for the experiments in which the eddies detached from the cape (Fig. 11a) and therefore by looking at the maxima of the autocorrelation functions it was possible to determine the rotation period of the vortices. This ranged between 18 and 36 s. The zonal and meridional functions were in phase indicating that the flow had an eddy structure, and the decrease of correlation with time indicated that this eddy was not stationary. The number of particle paths extending for at least $\Delta t = 60$ s during the tracking process was too small for realistic values of autocorrelation to be calculated.

For the experiments in which $s > s'/\pi$ the vortex did not detach from the cape (Fig. 12). The maximum anticyclonic vorticity occurred at the center of the vortex and decreased outward. The continuous inflow from the current was balanced both by fluid leaking westward, as discussed in section 5a and visible in Fig. 12, and by fluid in the outer edge of the buoyant current that reattached to the cape and flowed along the side boundaries.


The autocorrelation (Fig. 11b) of the zonal (29) and meridional (30) components of the velocity for the case shown in Fig. 12 showed that the two functions were in phase, indicating the presence of an eddy structure. The main difference with Fig. 11a is that the autocorrelation did not decrease as much as in the eddy-shedding case, suggesting that the eddy was almost steady and that the westward drift was absent. After $\Delta t = 72$ s, realistic values of autocorrelation cannot be

calculated for the same reason mentioned above. For these experiments the rotation period of the eddy varied between 28 and 52 s.

c. Limits of the approximations made in the scaling analysis and comparison with experimental results

In [section 3](#) we assumed that the current was in geostrophic balance and we obtained the maximum vortex depth, supposed to be equal to the maximum current depth, as in [\(4\)](#). We measured the depth of the vortices by looking at the side view during the experiments and compared the value of the flow rate Q , as in [\(3\)](#) for a current in geostrophic balance, with the constant value of the variable Q utilized in the experiments. The values obtained with [\(3\)](#) ranged between 9 and 48 cm³ s⁻¹, which are large compared with $Q = 8.7$ cm³ s⁻¹ used in the experiments. A possible explanation is that the source of the current was a turbulent jet of buoyant water that retains some momentum after reaching the cape and therefore it did not develop into a completely buoyancy-driven current along the cape. A confined jet source of buoyant fluid will spread at first like a pure jet, but when the momentum generated by buoyancy comes to dominate over the initial momentum, the rate of spread becomes smaller and approaches that of a buoyancy-driven current. The distance L_j at which the buoyancy flux $B = g'Q$ dominates over the initial momentum flux $M = QU = Q^2/A$, where A is the area of the nozzle, can be calculated as ([Turner 1973](#))

$$L_j = 1.85 \frac{M^{3/4}}{B^{1/2}}, \quad (31)$$


and in an actual experiment L_j is approximately 22 cm. Therefore, when the current encounters the cape 14 cm after the source, the initial momentum still dominates the buoyancy forces. In order to estimate the flow rate Q reaching the cape that is involved in the generation of the eddies, we assumed conservation of buoyancy flux Qg' between the source and the cape. The buoyant water from the source was characterized by $g' = 1.00$ cm s⁻², while the buoyant water in the vortex was characterized approximately by $g' = 0.60$ cm s⁻²; therefore, in order to conserve the buoyancy flux the flow rate at the cape was $Q_{\text{cape}} = 1.66Q$. The separation and reattachment of the current from the cape generated a vortex with a radius two or three times bigger than the Rossby radius of deformation $R_D = (g'(h_v h_2)^{1/2})^{1/2}/f$ calculated using the measured depth of the vortices ([Fig. 13](#) ). Hence R_D is a reasonable approximation for the radius.


In view of these considerations we restate here the values of the formation timescale t_f and drift timescale t_d . We consider the radius of the vortex to be equal to the Rossby radius of deformation calculated using the measured depth of the vortices, and in [\(5\)](#) we substitute $Q = Q_{\text{cape}}$ to give

$$t_f = \frac{\pi g' h_v \sqrt{h_v h_2}}{2f^2 1.66Q}. \quad (32)$$

In [\(6\)](#) we replaced the long Rossby wave speed with the westward drift velocity given by [\(26\)](#) to give

$$t_d = \frac{(g' \sqrt{h_v h_2})^{1/2}}{g' s \frac{\sqrt{h_v h_2}}{h_0} \left[1 + \frac{1}{2} \left(\frac{h_v}{h_0} \right) \right]}. \quad (33)$$

The regime diagram ([Fig. 14](#) ) shows that eddy shedding was observed for $t_f \leq t_d$ while for $t_f > t_d$ the eddy did not detach from the cape, consistent with our prediction from the scaling analysis in [section 3](#).

We also compared the measured time for the eddy to form, detach, and drift for a distance equal to 4 Rossby radii of deformation (approximately 2 radii of the eddy) with the value obtained using [\(32\)](#) and [\(33\)](#). The results in [Fig. 15](#)  suggest that the scaling analysis adopted in [section 3](#) is correct and show that the timescales in the transient regime are much larger than from the eddy-shedding regime, as anticipated in [section 5a](#).

Furthermore in [section 4b](#) we assumed that the eddy at the cape was generated by an inflow from the coastal current having zero potential vorticity. In order to verify its validity we measured the relative vorticity and compared it with the value

of the Coriolis parameter. If we assume that the eddies are in solid body rotation (see [section 6b](#)), the relative vorticity is given by $2\omega = 4\pi/T$, where T is the rotation period of the vortex. The results ([Fig. 16](#)) suggest that for values of f approximately less than 0.8 s^{-1} the absolute value of the vorticity is almost equal to the Coriolis parameter while the absolute value of the vorticity is approximately half the value of f when the latter is larger than 0.8 s^{-1} .

7. Comparison with observation of meddy formation

A major field program, called A Mediterranean Undercurrent Seeding Experiment (AMUSE), has been carried out to directly observe meddy formation and the spreading of Mediterranean Water (MW) into the North Atlantic ([Bower et al. 1997](#)). Between May 1993 and March 1994, nine meddy formation events were observed in the float trajectories, six near Cape St. Vincent, at the southwestern corner of the Iberian Peninsula, and three near the Estremadura Promontory, along the western Portuguese slope. The continental slope is quite steep between the launch site and Cape St. Vincent (5%–7%). Meddy formation thus occurs where the continental slope turns sharply to the right (when facing the downstream direction of the undercurrent) and the same conclusion was drawn from the investigation of a buoyant surface current flowing around a cape: anticyclonic vortices form at the cape when the boundary wall turns sharply to the right. The eddy-shedding mechanism described in this section and the meddy formation events have several characteristics in common.

First, one of the features of the formation events observed at Cape St. Vincent was how quickly the newly formed meddies were advected away from the formation site, thus terminating the formation process. For example, the meddy floats passed from boundary-following flow to anticyclonic looping, indicating that the formation was under way, in about 3–7 days. Furthermore, during or after the float made its first loop, the meddies were advected away from the formation site, indicating the termination of the formation process. The eddy shedding mechanism described in [section 3](#) suggests that eddy shedding occurs when the formation timescale is of the same order or smaller than the drift timescale and, therefore, could be a possible explanation for the mechanism that advected the observed meddies away from the formation site. Using a MW volume transport in the Gulf of Cadiz of 1.4–2.9 Sv ($\text{Sv} \equiv 10^6 \text{ m}^3 \text{ s}^{-1}$) and the observed dimension of meddies formed at the cape during the AMUSE and the Cadiz experiment [radius $\approx 15 \text{ km}$, thickness $\approx 0.65 \text{ km}$ ([Prater and Sanford 1994](#))], the value of $t_f = V/Q$ for the observed meddies would be about 1.1–2.3 days, shorter than the 3–7 days that was observed. This suggests that probably even less of the MW is involved in meddy formation. These values are of the same order as the drift timescale $t_d = R/U_d$ (3–4 days for meddies drifting at a velocity $U_d = 5 \text{ cm s}^{-1}$). Interestingly, during the AMUSE experiment the largest meddy was observed to form near Estremadura Promontory (radii larger than 20 km) and this particular meddy never detached from the boundary during the observational period of AMUSE. The larger radii suggest a formation timescale longer than for the other meddies and possibly longer than the drift timescale, hence this meddy would not be likely to detach and shed from the promontory.

Second, after leaving the formation site, meddies were observed to travel mainly along slope ([Figs. 7](#), [9](#) and [10](#) ([Bower et al. 1997](#))) and this characteristic was common to the eddies shed from the cape described in [section 5](#). This feature suggests that the topography plays a fundamental role in the formation and initial advection of the meddies and a westward drift due to the influence of a planetary β effect is not evident in these observations of meddies where floats ended up in cores of meddies only along the continental slope and not in deep water away from the slope. Third, meddies seem to form at Cape St. Vincent when the undercurrent is flowing strongly westward; a downstream speed greater than 12 cm s^{-1} in the undercurrent south of Portugal appears to be a necessary condition (not a sufficient condition though). As discussed in [section 6c](#) the use of a turbulent jet as a source of buoyant water allowed the current to retain some momentum after reaching the cape and to flow strongly around the cape. In some preliminary experiments we tested a lower value of the flow rate through the jet and utilized a simple point source of buoyant fluid instead of the jet source. In both of these experiments the absence of large momentum, and therefore of relatively fast current, arrested the formation and shedding of eddies from the cape in a similar fashion as in the observations of meddy formation at Cape St. Vincent. A fourth characteristic in common is the relative vorticity of these vortices. Meddies had a rotation period of 3–5 days, corresponding to relative vorticity between -5.0 and $-2.8 (\times 10^{-5} \text{ s}^{-1})$, or $-0.6f$ and $-0.3f$. For the experiments in which $t_f \leq t_d$ a rotation period between 18 and 36 s gave a relative vorticity between -0.7 s^{-1} and -0.3 s^{-1} ([Fig. 16](#)), or $-0.6f$ and $-0.4f$ (with the exception of two experiments). For the experiments in which $t_f > t_d$ a rotation period of 28–52 s gave a relative vorticity ranging almost as before between -0.7 s^{-1} and -0.2 s^{-1} ([Fig. 16](#)) but now corresponding to $-f$ and $-0.7f$ (with the exception of one experiment). The meddies and the shedding eddies observed in the laboratory ($t_f \leq t_d$) have the same relative vorticity when nondimensionalized with the planetary vorticity, indicating that these laboratory experiments provide a good simulation at smaller scale of what is happening in the real site, hence giving insights about the mechanism involved in the formation and drift of meddies. To reinforce this point we also compare the timescale of 5–9 rotation periods observed in the laboratory for the eddy to form, detach, and drift for a distance equal to four Rossby radii of deformation (see [section 6c](#)) with the timescale of about 3–7 days for a meddy to form and be advected away from the formation site. Again there is a good agreement between the laboratory experiments and the observation.

Finally, [Bower et al. \(1997\)](#) found that some of the anticyclonic relative vorticity of the meddies could come from anticyclonic shear in the undercurrent and suggested a formation mechanism most like that described by [D'Asaro \(1988\)](#), which relies on frictional torque along a boundary to generate the low potential vorticity found in the core of submesoscale coherent vortices. The expected radius of meddies formed by separation of the frictional boundary layer would be of the order of the width of the boundary layer, estimated to be around 10 km. The observed radius of meddies was usually larger than this value. The boundary layer width ([Stewartson 1957](#)) in the laboratory experiments was very small (between 0.4 and 1.3 cm) and, therefore, the determination of the anticyclonic shear of the buoyant current was not possible with the visualization technique used. However, the eddies again had a radius much larger than the boundary layer width, suggesting that the D'Asaro mechanism could account for the separation and reattachment of the flow around the cape and subsequent initial formation of anticyclonic vorticity, but the complete formation of the eddy and its possible detachment from the cape could be explained with the shedding mechanism described in [section 3](#).

8. The planetary β effect

Within the context of the homogeneous (one-layer) model there is a dynamical equivalence between the variation of the Coriolis parameter with latitude (the β effect) and variation of depth in the presence of constant f (for small bottom slopes and small Rossby number). Hence the value of β is replaced by sf/h_0 . The relative magnitudes of the relative vorticity gradient and the planetary vorticity gradient are measured by the parameter $U/\beta L^2$, where U and L are characteristic velocity and length scales, respectively.

In order to investigate the importance of the planetary β effect on the formation and drift of eddies in the oceans we performed some experiments with values of the slope that reproduced in the laboratory a flow dynamically equivalent to a flow influenced by the planetary variation of the Coriolis parameter. We assumed that the ratio of the relative vorticity gradient and the planetary vorticity gradient is the same in both the laboratory experiments and the oceans, namely

$$\frac{U_{2d}}{\beta_{\text{LAB}} R^2} = \frac{U_{\text{ocean}}}{\beta_{\text{plan}} L_{\text{ocean}}^2}, \quad (34)$$

where $\beta_{\text{LAB}} = sf/h_0$. Meddies have been observed ([Armi and Zenk 1984](#)) drifting at a velocity $U_{\text{ocean}} = 5 \text{ cm s}^{-1}$ and have a diameter of approximately 100 km. Considering $\beta_{\text{plan}} = 1.57 \times 10^{-13} \text{ cm}^{-1} \text{ s}^{-1}$ (corresponding to latitude 45° and a planetary radius of 6370 km), $U_{2d} = 0.17 \text{ cm s}^{-1}$, $R = 6 \text{ cm}$, $f = 1.37 \text{ s}^{-1}$, and $h_0 = 15 \text{ cm}$, the value of the slope from [\(34\)](#) is given by $s = 0.05$. We carried out two experiments, with $s = 0.05$ and $s = 0.10$, and compared them with the corresponding experiments with the same value of f and a larger value of the slope. For both values of the slope a vortex was observed forming at the cape by the usual mechanism. However, the vortex did not detach nor drift from the cape and behaved in a similar way to the case presented in [section 5a](#) for $s > s'/\pi$.

9. Conclusions

Laboratory experiments were performed to investigate a buoyant current flowing along a side boundary and around a cape over a sloping bottom. They showed how a vortex can be generated from the current where it separates and reattaches to the cape and that, under some conditions, the eddy is able to detach from the cape and drift westward following isobaths. Two important timescales regulate the flow: the time t_f that the current takes to generate a vortex and the time t_d that the vortex takes to drift westward for a distance equal to its radius. When these two timescales are similar or $t_f < t_d$, the eddy was observed to translate westward with approximately the same theoretical speed found in [section 4](#). For $t_f > t_d$ the vortex was able to form at the cape but it did not detach nor drift westward. The influence of the depth of the lower layer, h_0 , on the flow was investigated. The eddy drift was observed for $h_0 = 14 \text{ cm}$, whereas an increase of the lower-layer depth to 25 cm completely inhibited the detachment and drift of the vortex from the cape. The deeper lower layer implies a slower westward speed, U_{2d} . The experiments, on the other hand, indicate that for sufficiently small values of the westward speed the whole process no longer takes place. The values of the slope s required in the experiments in order to obtain the detachment and drift of the vortex indicate that the phenomena will occur on a planetary β plane only when the variation of the Coriolis parameter with latitude is reinforced by a topographic β effect. This suggests that only peninsulas or capes on a sufficiently steep shelf (so that $s \geq 0.25$ but still $s \leq s'/\pi$) can cause the detachment and drift of a vortex from a boundary current.

Different orientations of the cape with respect to the isobaths show that eddies only drift westward, if the geometry allows this, and the behavior of the drifting eddies is similar for different orientations of the cape. Finally, we investigated the

loss of coherence and destruction of the anticyclonic eddies before they could reach the western wall of the tank. An active (shallow) lower layer led to instability of both the boundary current and the anticyclonic eddy. Cyclones were generated in the lower layer. These were advected to deeper water by interaction with the anticyclonic eddies, increasing their intensity until they destroyed the anticyclones. The precise nature of the instability was difficult to determine because both baroclinic and barotropic instabilities present many features in common.

This study suggests that the formation, detachment, and drift of an eddy from a current flowing around a cape is a delicate process that takes place only if the water depth is not too deep and the topography is steep enough (so that $0.25 \leq s \leq s'/\pi$). The orientation of the cape must also allow the westward motion of the vortex (i.e., the coastline is not directly westward of the cape). These conditions appear to be satisfied, for example, in the Canary Basin, where the Mediterranean outflow from the Strait of Gibraltar flows along the coast of Spain and around Cape St. Vincent. A good agreement between the laboratory experiments and the observations of meddies in that region suggests that an eddy-shedding process similar to that observed in the laboratory experiments takes place.

Acknowledgments

We wish to thank the staff of the GFD summer study program for providing a stimulating environment during the summer, and especially George Veronis and Ross Griffiths for their suggestions and advice and Doron Nof for initial encouragement. A special thanks to John Salzig for providing assistance and help to make the experiments possible. Support from NSF under Grants OCE-9314484 and OCE-9633063 and from TMR Fellowship MAS3-CT96-5017 is also acknowledged.

REFERENCES

- Armi, L., and W. Zenk, 1984: Large lenses of highly saline Mediterranean water. *J. Phys. Oceanogr.*, **14**, 1560–1576. [Find this article online](#)
- , D. Herbert, N. Oakey, J. Price, P. Richardson, T. Rossby, and B. Ruddick, 1988: The history and decay of a Mediterranean salt lens. *Nature*, **333**, 649–651.
- Bjerknes, J., and J. Holmboe, 1944: On the theory of cyclones. *J. Meteor.*, **1**, 1–22.
- Bower, A. S., L. Armi, and I. Ambar, 1997: Lagrangian observation of Meddy formation during a Mediterranean undercurrent seeding experiment. *J. Phys. Oceanogr.*, **27**, 2545–2575. [Find this article online](#)
- Cenedese, C., and P. F. Linden, 1999: Cyclones and anticyclone formation in a rotating, stratified fluid over sloping bottom topography. *J. Fluid Mech.*, **381**, 199–223.
- Cushman-Roisin, B., 1994: *Introduction to Geophysical Fluid Dynamics*. Prentice-Hall, 320 pp.
- , E. P. Chassignet, and B. Tang, 1990: Westward motion of mesoscale eddies. *J. Phys. Oceanogr.*, **20**, 758–768. [Find this article online](#)
- D'Asaro, E. A., 1988: Generation of submesoscale vortices: A new mechanism. *J. Geophys. Res.*, **93**, 6685–6693.
- Dalziel, S. B., 1992a: DigImage: System overview. Cambridge Environmental Research Consultants, Ltd., 43 pp. [Available from Cambridge Environmental Research Consultants, Ltd., 3 King's Parade, Cambridge CB2 1SJ, United Kingdom.]
- , 1992b: Decay of rotating turbulence: Some particle tracking experiments. *Appl. Sci. Res.*, **49**, 217–244.
- , 1993: Rayleigh–Taylor instability: Experiments with image analysis. *Dyn. Atmos. Oceans*, **20**, 127–153.
- Davey, M. K., and P. D. Killworth, 1989: Flow produced by discrete sources of buoyancy. *J. Phys. Oceanogr.*, **19**, 1279–1290. [Find this article online](#)
- Griffiths, R. W., and P. F. Linden, 1981: The stability of vortices in a rotating, stratified fluid. *J. Fluid Mech.*, **105**, 283–316.
- , and E. J. Hopfinger, 1986: Experiments with baroclinic vortex pairs in a rotating fluid. *J. Fluid Mech.*, **173**, 501–518.
- , and —, 1987: Coalescing of geostrophic vortices. *J. Fluid Mech.*, **178**, 73–97.
- Jiang, L., and R. W. Garwood Jr., 1996: Three-dimensional simulation of overflows on a continental slope. *J. Phys. Oceanogr.*, **26**, 1214–

Jungclaus, J. H., 1999: A three-dimensional simulation of the formation of anticyclonic lenses (meddies) by the instability of an intermediate depth boundary current. *J. Phys. Oceanogr.*, **29**, 1579–1598.. [Find this article online](#)

Linden, P. F., 1991: Dynamics of fronts and eddies. *Nonlinear Topics in Ocean Physics: Proc. of the Enrico Fermi Summer School*, A. Osborne, Ed., Elsevier Science, 313–351..

—, B. M. Boubnov, and S. B. Dalziel, 1995: Source–sink turbulence in a rotating stratified fluid. *J. Fluid Mech.*, **298**, 81–112..

Mory, M., 1985: Integral constraints on bottom and surface isolated eddies. *J. Phys. Oceanogr.*, **15**, 1433–1438.. [Find this article online](#)

—, M. E. Stern, and R. W. Griffiths, 1987: Coherent baroclinic eddies on a sloping bottom. *J. Fluid Mech.*, **183**, 45–62..

Nof, D., 1983: The translation of isolated cold eddies on a sloping bottom. *Deep-Sea Res.*, **30**, 171–182..

Pedlosky, J., 1979: *Geophysical Fluid Dynamics*. Springer, 624 pp..

Pichevin, T., and D. Nof, 1996: The eddy cannon. *Deep-Sea Res.*, **43**, 1475–1507..

Pingree, R. D., and B. Le Cann, 1993: Structure of a meddy (Bobby 92) southeast of the Azores. *Deep-Sea Res.*, **40**, 2077–2103..

Prater, M. D., and T. B. Sanford, 1984: A meddy off Cape St. Vincent. Part I: Description. *J. Phys. Oceanogr.*, **24**, 1572–1586.. [Find this article online](#)

Rossby, C. G., 1948: On displacements and intensity changes of atmospheric vortices. *J. Mar. Res.*, **26**, 175–187..

Stern, M. E., 1975: Minimal properties of planetary eddies. *J. Mar. Res.*, **33**, 1–13..

Stewartson, K., 1957: On almost rigid rotation. *J. Fluid Mech.*, **3**, 17–26..

Swaters, G. E., 1991: On the baroclinic instability of cold-core couple density fronts on a sloping continental shelf. *J. Fluid Mech.*, **224**, 361–382..

Turner, J. S., 1973: *Buoyancy Effects in Fluids*. Cambridge University Press, 367 pp..

Whitehead, J. A., M. E. Stern, G. R. Flierl, and B. A. Klinger, 1990: Experimental observations of baroclinic eddies on a sloping bottom. *J. Geophys. Res.*, **95**, 9585–9610..

APPENDIX

10. Induced Vorticity Drift

If vertical stretching and squashing dominates the make up of potential vorticity in the columns advected downslope and upslope, changes in relative vorticity are given by

$$\zeta = \mp \frac{sRf}{h_0}, \quad (\text{A1})$$

anticyclonic to the north and cyclonic to the south. Over a lengthscale of the Rossby radius of deformation the induced circulation (integrated vorticity) is

$$\Gamma = \frac{sR^3f}{h_0}, \quad (\text{A2})$$

and the center of the eddy at a distance R from these regions of positive and negative vorticity is subjected to an entraining velocity

With anticyclonic vorticity to the north and cyclonic vorticity to the south this entrainment velocity is directed westward and has exactly the same expression of (25) found in section 4c.

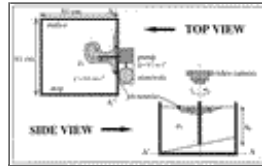
Tables

Table 1. Overview of experimental parameters (columns 2–5) and measured quantities (columns 6–9). The reduced gravity $g' = 0.60 \text{ cm s}^{-2}$ and the flow rate $Q = 8.7 \text{ cm}^3 \text{ s}^{-1}$ are the same for all experiments. Column 10 indicates the eddy-shedding region (0) for $s \leq s'/+\pi$; no eddy shedding (1) was observed for $s > s'/\pi$, while 2 indicates experiments in the transient regime, where the eddy shedding occurred after timescales much longer than in the region where $s \leq s'/\pi$. Asterisks denote experiments used in section 8 and double asterisks denote experiments used in section 5c. Blanks indicate quantities not measured.

Expts.	s	s'/π	h_0 (mm)	f (s ⁻¹)	$2R$ (mm)	U_{in} (cm s ⁻¹)	h_e (mm)	T (s)	Kind
6	0.50	0.62	14.0	0.81	13.6	0.12	6.0	0	
9	0.50	0.39	15.8	0.60	13.6	0.22	7.5	30.0	1
10	0.50	0.60	15.0	1.06	13.6	0.12	7.5	27.6	0
11	0.50	0.33	16.0	0.54	14.8	0.17	9.0	18.0	0
12	0.76	1.01	14.2	1.13	11.4	0.19	8.0	18.0	2
13	0.76	1.31	14.8	1.37	11.4	0.17	9.0	18.0	0
14	0.76	0.79	15.4	0.89	11.6	0.19	8.0	18.0	2
15	0.26	0.10	14.5	0.22	23.8	0.12	9.0	42.0	1
16	0.26	0.29	15.1	0.48	19.0	0.12	8.0	27.6	0
17	0.26	0.47	15.5	0.68	16.7	0.14	6.0	36.0	0
21	0.76	0.41	14.7	0.61	12.2	0.14	8.0	21.6	2
22	0.76	0.15	15.5	0.31	11.4	0.17	6.5	40.8	2
23	0.50	0.10	15.5	0.22	11.6	0.17	5.0	40.8	1
24	0.50	1.20	15.1	1.30	10.2	0.16	7.0	21.6	0
25	0.26	0.75	15.3	0.94	12.5	0.13	6.5	25.6	0
26	0.26	1.01	16.7	1.18	11.4	0.17	6.0	21.6	0
30	0.50	0.10	15.7	0.22	11.6	0.17	4.0	40.8	1
36	0.00	0.77	17.8	1.00	13.8	0.17	7.5	30.0	*
37	0.00	0.20	15.5	0.50	16.8	0.17	5.5	30.0	*
38	0.00	0.11	16.4	0.25	25.0	0.17	4.0	30.0	*
39	0.11	0.29	15.0	0.48	20.0	0.08	4.5	30.0	*
40	0.05	1.30	15.0	1.37	10.0	0.17	5.0	30.0	*
41	0.76	0.77	22.8	1.06	17.6	0.17	5.5	30.0	**
42	0.76	1.03	22.9	1.30	6.5	0.17	5.0	30.0	**
43	0.76	0.10	16.2	0.22	16.2	0.17	4.0	30.0	1
49	0.62	1.06	15.8	1.20	10.7	0.17	10.5	20.4	0
50	0.62	1.10	14.3	1.20	10.7	0.22	9.5	20.4	0
51	0.62	0.79	14.8	0.96	11.9	0.18	9.5	24.0	0
52	0.62	0.69	13.6	0.71	11.1	0.11	6.5	24.0	2
53	0.62	1.31	14.6	1.37	9.5	0.23	9.5	24.0	0
55	0.38	0.74	15.5	0.94	10.7	0.16	6.5	24.0	0
56	0.38	0.44	16.0	0.65	13.5	0.19	7.5	21.6	0
57	0.38	0.15	15.3	0.31	19.1	0.16	7.0	21.6	1
58	0.38	1.02	16.0	1.18	11.9	0.19	8.0	24.0	0

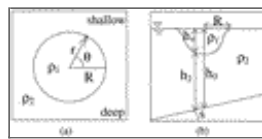
Click on thumbnail for full-sized image.

Figures



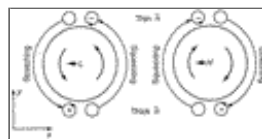
Click on thumbnail for full-sized image.

Fig. 1. Sketch of the experimental apparatus. Arrows denote the flow direction.



Click on thumbnail for full-sized image.

Fig. 2. Schematic diagram of the eddy over a sloping bottom: (a) top view and (b) side view.



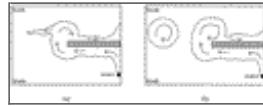
Click on thumbnail for full-sized image.

Fig. 3. Sketch illustrating the β gyre approach in order to explain the vortex westward drift. The advection of surrounding fluid induces cyclonic and anticyclonic vorticities, which combine to induce a drift of the vortex structure along lines of constant thickness. In the Northern Hemisphere (as drawn in figure), the vortex moves with the thin-layer side on its right; the direction is opposite in the Southern Hemisphere (Cushman-Roisin 1994).



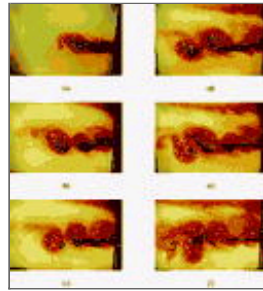
Click on thumbnail for full-sized image.

Fig. 4. Regime diagram illustrating the eddy-shedding region (open diamonds) for $s \leq s'/\pi$. No eddy shedding (solid diamonds) was observed for $s > s'/\pi$. Solid triangles indicate experiments in the transient regime where the eddy shedding occurred after timescales much longer than in the region where $s \leq s'/\pi$.



Click on thumbnail for full-sized image.

Fig. 5. Sketch illustrating the eddy not shedding from the cape (a) for $s > s'/\pi$, and the eddy shedding from the cape (b) for $s \leq s'/\pi$.



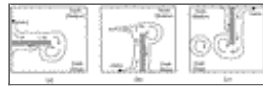
Click on thumbnail for full-sized image.

Fig. 6. Formation (a) and westward drift (b, c, d, e) of anticyclonic baroclinic vortices from a buoyant surface current flowing along a side boundary and around a cape for $f = 0.96 \text{ s}^{-1}$, $s = 0.62$, $s'/\pi = 0.79$, and $h_0 = 14.8 \text{ cm}$. The anticyclone was unstable (e) and formed two spiral arms as a result of the generation of cyclonic vorticity in the lower layer by baroclinic instability. The lower-layer flow was seen by injecting dye (see as the darker tracer) in the southeast side of the cape: (a) after 3.8 rotation periods, (b) after 8.7 rotation periods, (c) after 10.8 rotation periods, (d) after 13.3 rotation periods, (e) after 15.9 rotation periods, and (f) after 19.5 rotation periods. The white particles in the panels are buoyant paper pellets added on the surface.



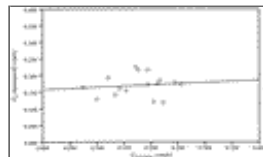
Click on thumbnail for full-sized image.

Fig. 7. Sketch illustrating the instability processes that originated on the (a) current and on vortex (b).



Click on thumbnail for full-sized image.

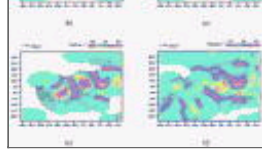
Fig. 8. Sketch illustrating the different orientations of the cape relative to the direction of the bottom slope.



Click on thumbnail for full-sized image.

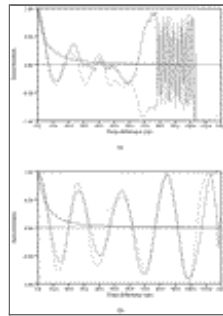
Fig. 9. The westward drift speed measured for the experiments in which $s \leq s'/\pi$, plotted against the predicted drift speed (26) calculated in [section 4c](#).





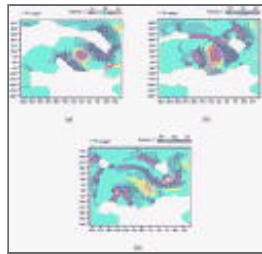
[Click on thumbnail for full-sized image.](#)

Fig. 10. Velocity and vorticity fields of anticyclonic baroclinic vortices shedding from a buoyant surface current flowing along a side boundary and around a cape for $t_f/t_d < 1$ (i.e., $s < s'/\pi$) for $f = 0.96 \text{ s}^{-1}$, $s = 0.62$, $s'/\pi = 0.79$, and $h_0 = 14.8 \text{ cm}$. The cape edge is positioned at $0, 0$: (a) after 3.8 rotation periods, (b) after 8.7 rotation periods, (c) after 10.8 rotation periods, (d) after 13.3 rotation periods, (e) after 15.9 rotation periods, and (f) after 19.5 rotation periods. White regions represent no data.



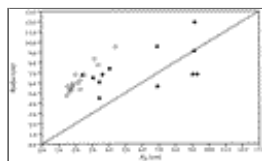
[Click on thumbnail for full-sized image.](#)

Fig. 11. Autocorrelation of the zonal (short dash) and meridional (long dash) component of the velocity for the experiment (a) in Fig. 10 and (b) in Fig. 12. The continuous line represents the fraction of the initial number of particles tracked for Δt to calculate the autocorrelation.



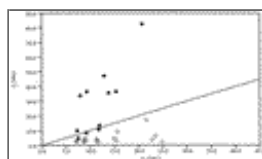
[Click on thumbnail for full-sized image.](#)

Fig. 12. Velocity and vorticity fields of anticyclonic baroclinic nonshedding vortices from a buoyant surface current flowing along a side boundary and around a cape for $t_f/t_d > 1$ (i.e., $s > s'/\pi$) for $f = 0.54 \text{ s}^{-1}$, $s = 0.50$, $s'/\pi = 0.33$, and $h_0 = 16.0 \text{ cm}$. The cape edge is positioned at $0, 0$: (a) after 3.8 rotation periods, (b) after 8.7 rotation periods, and (c) after 10.8 rotation periods. White regions represent no data.



[Click on thumbnail for full-sized image.](#)

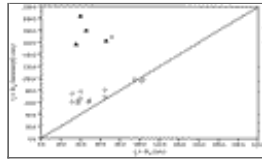
Fig. 13. The measured eddy radius vs the Rossby radius of deformation calculated using the measured depth of the vortices. Radius of nonshedding (solid diamonds) and shedding (open diamonds) eddies and of eddies in the transient regime (solid triangles).



[Click on thumbnail for full-sized image.](#)

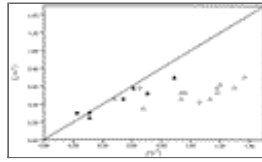
Fig. 14. Regime diagram illustrating the eddy-shedding region (open diamonds) for $t_f \leq t_d$. No eddy shedding (solid diamonds) was observed for $t_f > t_d$. The solid triangles indicate experiments in the transient regime where eddy shedding

occurred after timescales much longer than in the region where $t_f \lesssim t_d$.



[Click on thumbnail for full-sized image.](#)

Fig. 15. Timescale for the eddy to form and detach to drift for a distance equal to 4 Rossby radii of deformation (approximately two radii of the eddy) vs $(t_f + 4t_d)$. Timescale for shedding eddies (open diamonds) and for eddies in the transient regime (solid triangles).



[Click on thumbnail for full-sized image.](#)

Fig. 16. Absolute value of the vorticity ζ vs the Coriolis parameter f for nonshedding (solid diamonds) and shedding (open diamonds) eddies and for eddies in the transient regime (solid triangles).

* Additional affiliation: Physical Oceanography Department, Woods Hole Oceanographic Institution, Woods Hole, Massachusetts.

Corresponding author address: Dr. Claudia Cenedese, Woods Hole Oceanographic Institution, MS#21, 360 Woods Hole Rd., Woods Hole, MA 02543. E-mail: ccenedese@whoi.edu

[top ▲](#)



© 2008 American Meteorological Society [Privacy Policy and Disclaimer](#)
Headquarters: 45 Beacon Street Boston, MA 02108-3693
DC Office: 1120 G Street, NW, Suite 800 Washington DC, 20005-3826
amsinfo@ametsoc.org Phone: 617-227-2425 Fax: 617-742-8718
[Allen Press, Inc.](#) assists in the online publication of AMS journals.